

Current gain and external quantum efficiency modeling of GeSn based direct bandgap multiple quantum well heterojunction phototransistor

Vedatrayee Chakraborty¹ · Swagata Dey¹ · Rikmantra Basu² ·
Bratati Mukhopadhyay¹ · P. K. Basu¹

Received: 28 July 2015 / Accepted: 13 February 2017 / Published online: 4 March 2017
© Springer Science+Business Media New York 2017

Abstract This paper aims to provide the performance characteristics of proposed, strain balanced direct band gap multiple quantum wells (MQWs) hetero phototransistor (HPT) made of SiGeSn/GeSn alloys grown on Si substrate which is compatible with recent CMOS fabrication technology. This also presents a comprehensive comparison of this proposed structure with the existing HPT structure made of indirect gap Ge/SiGe MQWs. Alloys of Ge and Sn grown on Si platform shows about tenfold increase in absorption over Ge at C and L-bands due to direct nature of band gap in GeSn. Initial work begins the solution of continuity equation to solve the different terminal current densities and optical gain of the multiple quantum well structure. Main analysis was concentrated on finding the external quantum efficiency depending on the doping variations of emitter and base, base width etc. Finally the photocurrent density variations are estimated for the structure and compared with existing indirect band gap HPT. The calculated values for direct band gap GeSn HPT device are found to be comparable with those for indirect band gap SiGe device to flourish as a potential candidate of photo detectors for the present day telecommunication network.

Keywords Hetero phototransistor · Ge/SiGe MQWs · Optical gain · QE

✉ Vedatrayee Chakraborty
vedatrayee_chakraborty@yahoo.co.in

Swagata Dey
swagata dey2009@gmail.com

Rikmantra Basu
rikmantrabasu@nitdelhi.ac.in

Bratati Mukhopadhyay
bmrp@caluniv.ac.in

P. K. Basu
pkbasu_rpe@yahoo.co.in

¹ Institute of Radio Physics and Electronics, University of Calcutta, Kolkata 700009, India

² ECE Department, National Institute of Technology Delhi, Delhi 110040, India

1 Introduction

Photonic devices using Si or group IV semiconductors on a Si platform are of immense interest as the devices may be monolithically integrated with Si CMOS circuits. Unfortunately however, it is difficult to realize such devices, in particular, light emitters and modulators due to the indirect nature of the band gap (Deen and Basu 2012; Pavesi and Lockwood 2004). In case of photodetectors also, the band gap of Si does not match the standard telecommunication wavelengths of 1300 and 1550 nm. Though the band gap of Ge is compatible, direct growth of Ge and its alloy, SiGe, on Si substrate results in several problems due to a large degree of lattice mismatch.

The scenario has changed significantly with the development of the alloys of Ge and Si with another gr. IV material Sn. A practical chemical vapour deposition technique (CVD) has been developed recently (Bauer et al. 2002; D'Costa et al. 2006; Roucka et al. 2008; Chizmeshy et al. 2006; Menendez and Kouvetakis 2004) that produces high quality GeSn thin film directly on a Si substrate. By varying the composition of Sn, these alloys may be lattice matched, strained or strain-balanced. A notable feature of the alloy or Ge is that the direct Γ valley of Ge and GeSn decreases rapidly with increasing tensile strain or increasing Sn concentration than the indirect L valley and thus there is an indirect to direct crossover. Direct gap type I heterostructures have been realized in tensile strained Ge using GeSiSn barriers. The developed alloys and heterojunctions are now being studied for application in lasers (Sun et al. 2010a, b; Chang and Chuang 2007; Zhu et al. 2010; Chang et al. 2010), modulators (Chakraborty et al. 2013; Schaevitz et al. 2012; Chang and Chang 2012; Moontragoon et al. 2010) and photodetectors.

There is growing interest to utilize the direct nature of the band gap of GeSn alloy for fabrication of photodetectors also. So far p-i-n detectors (Oehme et al. 2012; Moontragoon et al. 2010) and photoconductive detectors (D'Costa et al. 2009; Su et al. 2011) are already reported by workers using large absorption coefficient of direct-gap GeSn alloys.

There is an attractive alternative to the p-i-n detectors and APDs in the form of Heterojunction Bipolar Phototransistors (HPTs). HPTs in three terminal configuration, provides internal gain but without any excess noise, which is a detrimental effect in APDs. A number of workers in past and recent times have studied the performance of HPTs (Scott and Fetterman 1995; Frimel and Roenker 1997a, b; Tan et al. 2005; Khan et al. 2011; Park and Jang 2010). However, most of the research has been performed with III-V compounds and alloys. In connection with gr. IV materials, there is a report by Zhang et al. (2008) on the numerical analysis of an HPT in which ten periods of Ge/Si_{0.4}Ge_{0.6} multiple Quantum Wells (MQWs) grown on a virtual SiGe substrate.

In view of the direct nature of GeSn alloy, it seems worthwhile to undertake detailed investigation of the use of GeSn and other alloys in HPT structures. In our previous work (Basu et al. 2013, 2014a, b) we have studied and calculated values of current gain, optical gain, spectral response and signal-to-noise ratio for GeSn based HPT devices and made comparison with the InP-InGaAs-InP HPTs and found that the GeSn-based HPTs can compete with InGaAs-based devices. This encourages us to study other configurations of GeSn based HPTs.

In this present work, we have considered a similar structure proposed by Zhang et al. (2008), but using a direct gap GeSn/Si GeSn type I MQWs, instead of the indirect gap Ge/SiGe MQWs considered by Zhang et al. Our structure considers a strain-balanced system in conformity with the structure considered by Chang et al. (2010) for the study of laser action. Strain relaxed buffers (SRB) act as "Virtual Substrates" (VS) on which the whole

material is grown. These SRB platforms can either support strained or relaxed layers, but should be relaxed so as not to generate crystal imperfections in the over layer during subsequent growth or processing. In our present model, the layers of HPT are grown on the GeSn virtual substrate and all the layers are considered as strain-free. Our analysis follows basically the theory developed by Zhang et al. (2008), but uses the material parameters appropriate for GeSn alloy. The absorption coefficient is calculated by using standard expression involving the momentum matrix element. We have compared our calculated values of photocurrent, current gain and quantum efficiency with the results obtained by Zhang et al. (2008) and has found significant improvement with respect to all characteristics.

Our structure is described in Sect. 2; the expressions used in our work, which are essentially developed by Zhang et al. (2008), are given in Sect. 3. The results are given in Sect. 4, describing their features; this section attempts to make a comparison between our results and the values obtained by Zhang et al. (2008). The conclusions are given in Sect. 5.

2 Structure

The structure considered in our present work is shown in Fig. 1 which is almost similar to the strain balanced structure referred in Chang et al. (2010). There is also a schematic band structure of the entire detector with carriers' movement shown in Fig. 1. A fully strain-relaxed $\text{Ge}_{0.88}\text{Sn}_{0.12}$ buffer layer of lattice constant 5.7571 \AA is grown on a (001)-oriented Si of 5.4307 \AA substrate to act as virtual substrate for the growth of all layers. Then an n-type $\text{Si}_{0.08}\text{Ge}_{0.78}\text{Sn}_{0.14}$ layer of 5.7556 \AA is grown on it and it acts as a collector. A ten periods of $\text{Ge}_{0.84}\text{Sn}_{0.16}/\text{Si}_{0.09}\text{Ge}_{0.8}\text{Sn}_{0.11}$ MQW (well is of 5.7904 \AA and barrier is of 5.7284 \AA) is grown on the collector contact. The lattice constant of the $\text{Ge}_{0.84}\text{Sn}_{0.16}$ wells is larger than that of that of the $\text{Ge}_{0.88}\text{Sn}_{0.12}$ buffer layer, includes a compressive strain in $\text{Ge}_{0.88}\text{Sn}_{0.12}$ wells. On the other hand, the $\text{Si}_{0.09}\text{Ge}_{0.8}\text{Sn}_{0.11}$ barriers have a smaller lattice constant than $\text{Ge}_{0.88}\text{Sn}_{0.12}$ buffer layer. So, tensile strain is generated which compensates

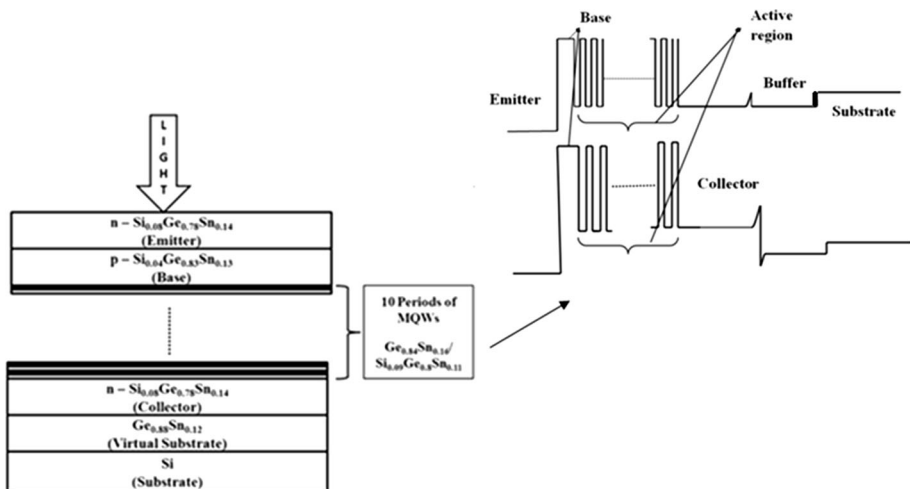


Fig. 1 Schematic band structure of the entire MQW HPT with carriers' movement

the compressive strain generated at wells as the both type of strains are of equal amount. The design of such alternating compressive-strained wells and tensile-strained barriers satisfy the strain balanced condition which in turns reduces the defects. A p-type base region is grown on it with $\text{Si}_{0.04}\text{Ge}_{0.83}\text{Sn}_{0.13}$ of 5.7564 Å. The emitter terminal is formed by a n-type $\text{Si}_{0.08}\text{Ge}_{0.78}\text{Sn}_{0.14}$ of 5.7556 Å which has a bandgap (0.5076 eV) greater than the bandgap of the material used for the base (0.4859 eV). As the bandgap of the emitter is higher than the bandgap of the base the structure becomes type I. Since $\text{Ge}_{0.88}\text{Sn}_{0.12}$ buffer layer is fully strain-relaxed, the lattice constants of the layers grown on it will be either compressed or extended equally. In this model structure a thick absorption layer is modeled by considering GeSn/SiGeSn MQW structure. This MQW absorption layer increases the light absorption significantly.

The biasing of HPT is same as of conventional n-p-n transistor. Here it is considered that the incident light passes through the wide-gap emitter and mainly absorbed by MQW absorption layer to generate electron-hole pairs. Electrons are swept to the collector because of reverse bias generating the initial photocurrent of HPT. Hole diffusion is occurred to the emitter base region. A large potential barrier exists in valence band between emitter and base junction which results an accumulation of hole. If the forward bias is increased, large amount of electron current flows from emitter to collector. The photocurrent at collector is significantly enhanced and higher external quantum efficiency can be obtained by this process.

3 Theory

We followed the analysis based on the method of Zhang et al. (2008) where a SiGe n-p-n HPT with MQWs is considered neglecting the effects of tunneling and minority carrier recombination. In our present work we have considered a N-p-N HPT model with GeSn/SiGeSn MQW absorption region.

Most of the parameters for binary and ternary alloy materials like lattice constants etc. are estimated using linear interpolation technique, as,

$$a_{\text{Si}_x\text{Ge}_y\text{Sn}_{1-x-y}} = x \times a_{\text{Si}} + y \times a_{\text{Ge}} + (1 - x - y)a_{\text{Sn}} \tag{1}$$

$$a_{\text{Ge}_z\text{Sn}_{1-z}} = z.a_{\text{Ge}} + (1 - z).a_{\text{Sn}} \tag{2}$$

In our model we have considered the light, having wavelength of 1.55 μm and of 1 μW power is incident on the top of the structure. Now solving the one dimensional diffusion equation for emitter region (Sun et al. 2010),

$$D_{pE} \frac{d^2 \Delta p_E}{dx^2} - \frac{\Delta p_E}{\Gamma_E} + g_E = 0 \tag{3}$$

where Δp_E is the excess hole concentration in the emitter, D_{pE} is hole diffusion coefficient and Γ_E is the hole minority carrier lifetime in the emitter.

Since the structure is front side illuminated so, the generation rate of hole caused by the optical incidence at emitter can be expressed as,

$$g_E = \eta_E \alpha_E F_0 \exp(-\alpha_E x) \tag{4}$$

where α_E is the optical absorption coefficient in the emitter, η_E is internal quantum efficiency and F_0 is the incident optical flux density at the surface of the emitter which can be

expressed as, $F_0 = \frac{P_0}{Ah\nu}$, where, P_0 is optical power, A is area of the emitter and $h\nu$ is the photon energy.

Finally the current density due to hole diffusion can be expressed as (Zhang et al. 2008),

$$J_{pE} = qD_E \frac{d\Delta p_E}{dx} \Big|_{x=W_E} = -G_E F_0 + J_{OpE} \left\{ \exp\left(\frac{qV_{BE}}{kT}\right) - 1 \right\} \tag{5}$$

where,

$$G_E = q\eta_E \frac{\alpha_E L_E}{1 - \alpha_E^2 L_E^2} \left\{ \left(\alpha_E L_E + \frac{\xi_2}{\xi_1} \right) \exp(-\alpha_E W_E) - \frac{1}{\xi_1} \left(\alpha_E L_E + \frac{s_E L_E}{D_E} \right) \right\} \tag{6}$$

and

$$J_{OpE} = q \frac{D_E \xi_2}{L_E \xi_1} p_E \tag{7}$$

$$\xi_1 = \cosh \frac{W_E}{L_E} + \frac{s_E L_E}{D_E} \sinh \frac{W_E}{L_E} \tag{8}$$

Similarly steady state excess electron concentration profile can be obtained for base region again by solving the diffusion equation for base region. The generation rate of electron induced by optical excitation at base would be,

$$g_B = \eta_B \alpha_B F_0 \exp(-\alpha_E W_E) \exp(-\alpha_B x) \tag{9}$$

The electron current density at the emitter end of the quasi-neutral base is (Zhang et al. 2008),

$$J_{nBE} = -qD_B \frac{d\Delta n_B}{dx} \Big|_{x=0} = G_B F_0 f_{nBE} + J_{0nB} \left\{ \exp\left(\frac{qV_{BE}}{kT}\right) - 1 \right\} \cosh \frac{W_B}{L_B} + 1 \tag{10}$$

where,

$$G_B = q \frac{1}{\sinh\left(\frac{W_B}{L_B}\right)} \frac{\eta_B \alpha_B L_B \exp(-\alpha_E W_E)}{1 - \alpha_B^2 L_B^2} \tag{11}$$

$$f_{nBE} = \cosh\left(\frac{W_B}{L_B}\right) - \alpha_B L_B \sinh \frac{W_B}{L_B} - \exp(-\alpha_B W_B) \tag{12}$$

and

$$J_{0nB} = q \frac{D_B}{L_B} \frac{1}{\sinh\left(\frac{W_B}{L_B}\right)} n_B \tag{13}$$

Similarly, the current density at the collector end of the quasi neutral base is given by (Zhang et al. 2008),

$$J_{nBC} = J_{0nB} \left\{ \exp\left(\frac{qV_{BE}}{kT}\right) - 1 + \cosh\left(\frac{W_B}{L_B}\right) \right\} - G_B F_0 f_{nBC} \tag{14}$$

where,

$$f_{nBC} = 1 - \left\{ \cosh\left(\frac{W_B}{L_B}\right) + \alpha_B L_B \sinh\left(\frac{W_B}{L_B}\right) \right\} \exp(-\alpha_B W_B) \tag{15}$$

As the base region of HPT is highly doped the total depletion region of HPT induced by the collector–base bias includes absorption region and collector depletion region. The expression of the photocurrent is given by,

$$J_{dpl} = F_0 G_{dpl} \tag{16}$$

The hole density at the collector region can be expressed as

$$J_{pc} = J_{pco} + G_c F_0 \tag{17}$$

where

$$G_c = q \frac{\eta_c \alpha_c L_c}{1 - \alpha_c^2 L_c^2} \left\{ \exp(-\alpha_E W_E - \alpha_B W_B - \alpha_i W_i - \alpha_C W_{BC}) \right\} \left[\frac{\chi_2}{\chi_1} - \alpha_C L_C + \frac{1}{\chi_1} \left(\alpha_C L_C - \frac{s_C L_C}{D_C} \right) \exp(-\alpha_C W_C) \right] \tag{18}$$

$$\begin{aligned} \chi_1 &= \cosh\left(\frac{W_C}{L_C}\right) + \frac{s_C L_C}{D_C} \sinh\left(\frac{W_C}{L_C}\right) \\ \chi_2 &= \sinh\left(\frac{W_C}{L_C}\right) + \frac{s_C L_C}{D_C} \cosh\left(\frac{W_C}{L_C}\right) \end{aligned} \tag{19}$$

It is seen in our model that five photocurrent components flow into the base region, $J_{nBE} + J_{pE}$ from emitter junction, J_{dpl} from depletion region and $J_{nBC} + J_{pC}$ from the collector junction. The total current density must be constant; so we can write

$$J_{pE} + J_{nBE} + J_{nBC} + J_{dpl} + J_{pC} = 0 \tag{20}$$

In order to analyze the performance of the HPT the relation between the current gain and external quantum efficiency is calculated.

The final expression for the common emitter current gain is obtained as (Zhang et al. 2008),

$$\beta = \frac{\alpha}{1 - \alpha} = \frac{\gamma}{1 + \gamma \left[\cosh\left(\frac{W_B}{L_B}\right) - 1 \right]} \tag{21}$$

where,

$$\gamma = \frac{j_{0nB}}{j_{0pE}} = \frac{\gamma_0 \left(\frac{s_1}{s_2}\right)}{\sinh\left(\frac{W_2}{L_2}\right)} \tag{22}$$

and

$$\gamma_0 = \frac{D_{nB} L_{pE} N_E}{D_{pE} L_{nB} N_B} \left(\frac{m_{nB}^* m_{pB}^*}{m_{nE}^* m_{pE}^*} \right) \exp\left(\frac{\Delta E_g}{k_B T}\right) \tag{23}$$

The external quantum efficiency is related with current gain with β by the following expression (Zhang et al. 2008),

$$\eta_{ex} = \frac{\beta}{q} \left\{ G_E + G_B \left[f_{nBE} - f_{nBC} \cosh\left(\frac{W_B}{L_B}\right) \right] + G_{dpl} \cosh\left(\frac{W_B}{L_B}\right) + G_C \cosh\left(\frac{W_B}{L_B}\right) + \frac{\beta}{q\gamma} (G_{dpl} + G_C - G_B f_{nBC}) \right\} \tag{24}$$

Now in order to analyze the performance of HPT specified in our model, we have calculated different dependencies like band gap, absorption coefficient, mobility of the carriers.

The method used for calculating the band edges and band offsets in different materials is based on the model solid theory developed by Van de Walle (31, 32), which has been used by Menendez et al. (2004) In this approach bandgaps, lattice constant, strain and other parameters of constituent materials are used by estimating through linear interpolation technique where bowing parameters are include during calculation. The following expressions for the band edges of strained active layer are obtained as (Menendez and Kouvetakis 2004),

$$E_{v\Gamma}(\text{active layer}) = -\frac{\Delta_0(\text{substrate})}{3} - \Delta E_{v,av}(\text{substrate}) - \frac{\Delta_0(\text{active layer})}{6} + \delta E_h^0 + \frac{1}{4} \delta E_{001} + \frac{1}{2} \sqrt{\left(\Delta_0(\text{active layer}) + \frac{1}{2} \delta E_{001} \right)^2 + 2(\delta E'_{001})^2} \tag{25}$$

$$E_{c\Gamma}(\text{active layer}) = E_{v\Gamma}(\text{active layer}) + E_0(\text{active layer}) + \delta E_h^{c\Gamma} \tag{26}$$

$$E_{cL}(\text{active layer}) = E_{v\Gamma}(\text{active layer}) + E_{ind}(\text{active layer}) + \delta E_h^{cL} \tag{27}$$

The absorption coefficient for direct transition as a function of photon energy $\hbar\omega$ can be written as (Tan et al. 2005),

$$\alpha(\hbar\omega) = \frac{q^2 (2m_r)^{3/2} (\hbar\omega - E_g)^{1/2}}{2\pi\epsilon_0 c \eta m_0^2 \hbar^2} \frac{1}{\hbar\omega} \langle |P_{cv}^2| \rangle \tag{28}$$

where q is the electronic charge, m_r is reduced mass and it is expressed as $m_r^{-1} = m_e^{-1} + m_h^{-1}$, m_e is effective mass for electrons, m_h is effective mass for holes, η is refractive index, ϵ_0 is permittivity of free space, c is velocity of light in free space, m_0 is free electron rest mass, h is Plank’s constant and E_g is the bandgap energy.

$\langle |P_{cv}|^2 \rangle$ ia the average of the squared momentum matrix element for transitions between Bloch states in the valance and conduction bands. We use the expression for $\langle |P_{cv}|^2 \rangle$ for unpolarized light, which isdefined as,

$$\langle |p_{cv}^2| \rangle = \frac{m_0^2 E_g (E_g + \Delta)}{3m_e (E_g + 2\Delta/3)} \tag{29}$$

To calculate all parameters here we also considered the composition of each material using Vegard’s Law. By using the equation of absorption co-efficient we obtain a plot about the nature of absorption co-efficient with changing the photon energy $\hbar\omega$. The estimation of the absorption coefficient is different for the MQW absorption layer as it includes the multiple no. of quantum wells (Khan et al. 2011). The optical absorption coefficient is given by,

$$\alpha(h\omega) = \frac{2\pi}{\hbar(c/\eta)} \left(\frac{eA_0}{m_0} \right)^2 \sum_{1,2} |p_{12}|^2 (f_1 - f_2) \delta(E_{12} - \hbar\omega) \tag{30}$$

where,

$$p_{12} = \left\langle l \left| \exp(-ik_{\lambda} \cdot r) \cdot \epsilon_{\lambda} \cdot p \right|^2 \right\rangle \tag{31}$$

and f_1 and f_2 are the Fermi occupational probabilities for electrons in the respective states. The analytical values of motilities for electrons and holes of $\text{Si}_{1-x}\text{Ge}_x$ are obtained from Zhang et al. (2008) and mobility for GeSn and SiGeSn are calculated by the help of linear interpolation method. The responsivity of the photo detector has been calculated using the relation (32)

$$R = \eta_{ex} \frac{q\lambda}{hc} \tag{32}$$

where η_{ex} is the quantum efficiency of the detector of given wavelength λ , q is the electronic charge, h is the Plank’s constant, and c is the velocity of light in vacuum.

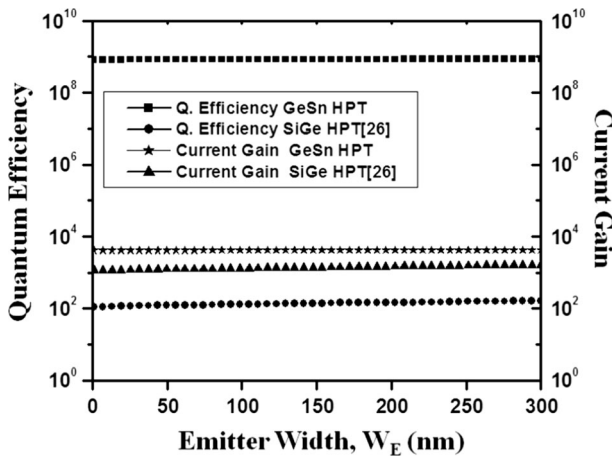


Fig. 2 External quantum efficiency and current gain variation with emitter width (W_E)

4 Results and discussion

The current gain and external quantum efficiency are calculated with different emitter widths for a fixed value of the emitter doping $N_E = 1 \times 10^{18} \text{ cm}^{-3}$. The values are plotted in Fig. 2 in which the data obtained by Zhang et al. (2008) are also included for comparison. Our simulation results could not be compared with experimental data as these are unavailable. It is hoped that the results presented in this work will stimulate experimental studies to verify the results and the use of the proposed structure for real life applications.

It is observed that the current gain increases slightly with increasing emitter width and that in turn increases the external quantum efficiency (QE). The increasing trend however is not significant in the logarithmic scale. The curves indicate that both the current gain and the quantum efficiency increase manifold in our structure from the respective values given by Zhang et al. (2008).

The effect of increment in emitter doping on current gain and QE is displayed in Fig. 3. With increasing emitter doping concentration (N_E), the injection efficiency increases which in turn increases the current gain as well as the external quantum efficiency. Both these quantities increase by few orders of magnitude in proposed GeSn device in comparison to the values given by Zhang et al. (2008) in SiGe HPT.

Base doping (N_B) and base width (W_B) also have an impact on HPT's performance as may be seen from the plots in Figs. 4 and 5 respectively. For a fixed base width, increasing base doping reduces the minority carrier life time and diffusion length, which results in decreasing current gain and the quantum efficiency as well. But highly doped base of the HPT provides a low base spreading resistance which increases the emitter base injection efficiency. This effect compensates the reducing effect of current gain and external efficiency. This phenomenon is considered as a major advantage of HPT. The decreasing nature of current gain and quantum efficiency with compared data are shown in Fig. 4.

From Eq. (19) it can be seen that the current gain is inversely proportional with base width where the base doping is kept fixed. This effect is plotted in Fig. 5. The quantum efficiency follows the similar nature of variation of current gain.

Photo current density in variation with base width and emitter widths are plotted in Figs. 6 and 7, respectively. The photocurrent density evolved due to diffusion of

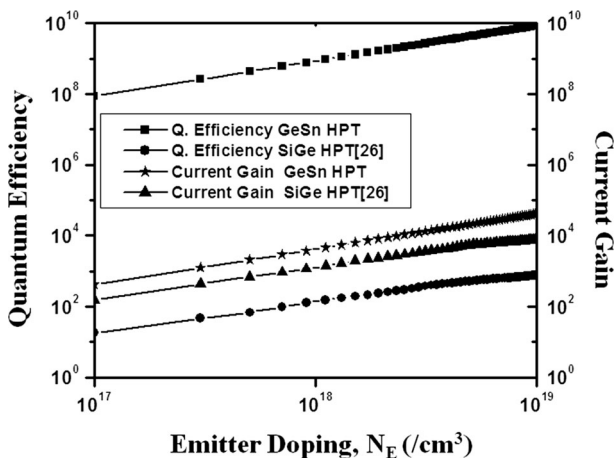


Fig. 3 External quantum efficiency and current gain variation with emitter doping concentration (N_E)

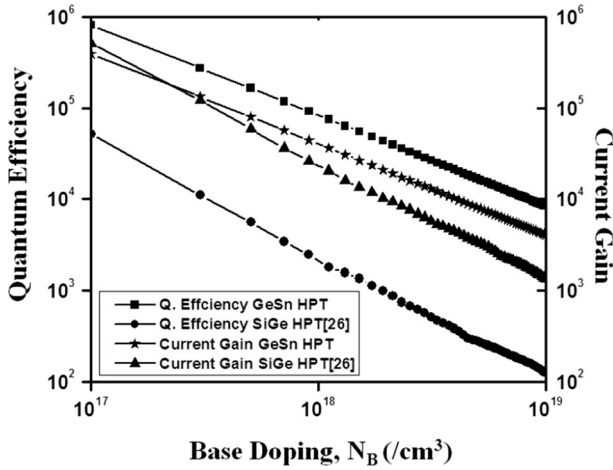


Fig. 4 External quantum efficiency and current gain variation with base doping concentration

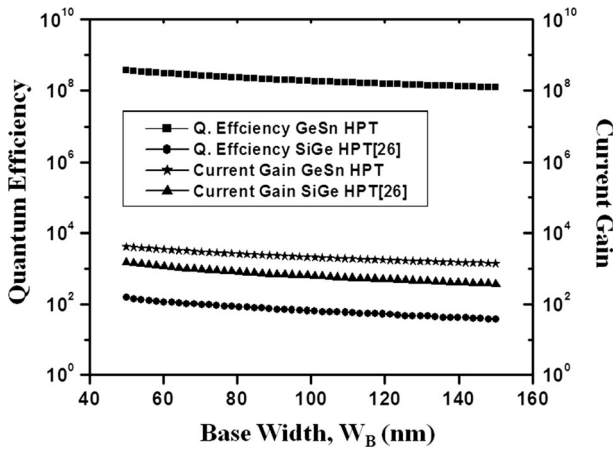


Fig. 5 External quantum efficiency and current gain variation with base width (W_B)

equilibrium holes in the emitter region (J_{ope}) and base region (J_{opb}) and the total photocurrent density (J_{dpi}) are included in the both the figures where the total photocurrent density includes the optical absorption in the depletion and collector regions. As the telecommunication range is taken as from 1300 nm to 1500 nm, the responsivity is calculated using the relation (32) and plotted with the variation of wavelength within this range. The results are plotted at Fig. 8. The result shows a decreasing effect. So, it can be concluded that device can be better operated at near infrared region.

An important Figure-of-merit of a photoreceiver is the Signal-to-ratio. We could not address this issue in the present work, as inclusion of the theory and method of calculation involved will shift the focus of the present paper to a widely different spot. In this

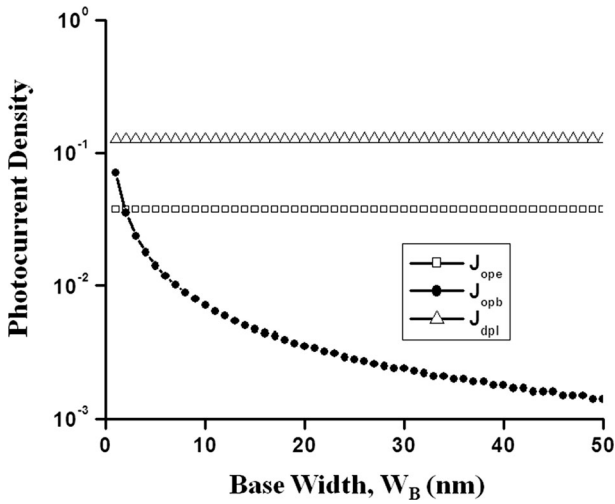


Fig. 6 Photocurrent density of each region variation with base width (W_B)

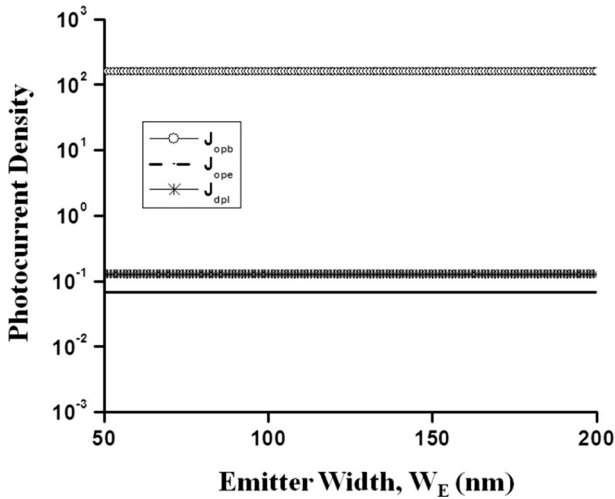
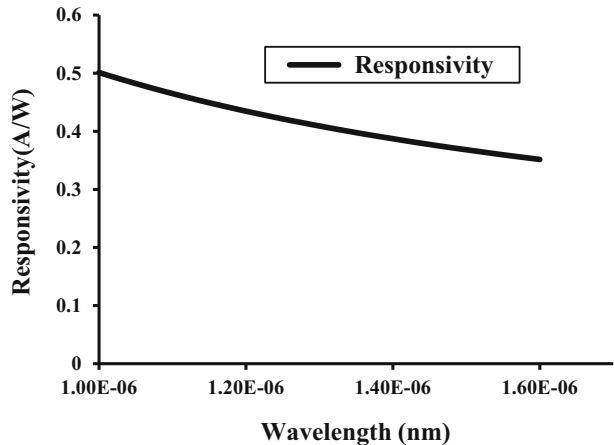


Fig. 7 Photocurrent density of each region variation with emitter width (W_E)

connection, it may be noted that SNR for a similar HPT as considered in the present work, but using a bulk GeSn in the base instead of the MQW has been calculated and reported in Basu et al. (2013). The calculated SNR has been found to increase with increasing input signal power. SNR value as large as 30 dB is obtained at 10 GHz with 0.1 μ W and 50 GHz with 1.0- μ W of the input power. Since gain increases by inserting MQWs in the base it may be expected that there may be a substantial increase in the SNR.

Fig. 8 Responsivity versus wavelength in the range of 1300–1600 nm



5 Conclusion

We have studied the performance of a N-SiGeSn/P-SiGeSn/N-SiGeSn HPT on a GeSn virtual substrate grown on Si. There are ten GeSn/SiGeSn types I MQWs in which the GeSn wells show direct band gap nature. The calculated values of current gain and quantum efficiency are order of magnitudes higher than the reported values for a similar strain balanced structure using Ge/SiGe MQWs, which increment perhaps, is due to the direct nature of the band gap of GeSn alloys. The highly improved performance of our HPT over the detector proposed by Zhang et al. (2008) is due to significantly larger absorption coefficient in GeSn QW possessing direct band gap. The dependence of current gain and QE on emitter and base doping and emitter and base widths are also studied. The results indicate that the present structure may be suitable as a photodetector operating in the 1550 nm range of fiber optic communication system. Appreciable values of the SNR in the photoreceiver using the present structure are expected. Similar work involved forms the subject of a separate paper, which will be published in near future.

The structure has the added advantage that it can be grown on Si and the process technology is compatible with the standard CMOS technology.

Acknowledgements The first author (VC) acknowledges supports from the UGC, New Delhi, India sponsored Project Fellowship under its RFSMS scheme and B.P. Poddar Institute of Management and Technology (ECE Dept). The second author (SD) acknowledges supports from the TEQUIP scheme.

References

- Basu, R., Chakraborty, V., Mukhopadhyay, B., Basu, P.K.: Predicted performance of Ge/GeSn hetero-phototransistors on Si substrate at 1.55 μm . *Opt. Quant Electron.* (2013). doi:10.1007/s11082-014-9921-3
- Basu, R., Chakraborty, V., Mukhopadhyay, B. and Basu, P. K.: Performance studies of a proposed Ge-GeSn-Ge heterojunction phototransistor and comparison with InGaAs-based Phototransistor. In: UK Semiconductors Conference 2014, University of Sheffield, UK, July 9–10, 2014a
- Basu, R., Chakraborty, V., Mukhopadhyay, B. and Basu, P. K.: Spectral and frequency response and signal to noise ratio of gesn-based heterojunction phototransistors. In: IEEE Photonics Conference 2014, (IEEE Photonics Society Annual Meeting) San Diego, CA, USA, October 12–26, 2014b. (Accepted for oral presentation)

- Basu, R., Chakraborty, V., Mukhopadhyay, B. and Basu, P. K.: Signal-to-noise ratio for a Ge-GeSn-GeSn hetero phototransistors at 1.55 μm , CODEC 2015, December, Swissotel, Kolkata
- Bauer, M., Taraci, J., Tolle, J., Chizmeshya, A.V.G., Zollner, S., Smith, D.J., Menendez, J., Hu, C., Kouvetakis, J.: Ge-Sn semiconductors for band-gap and lattice engineering. *Appl. Phys. Lett.* **81**(1–3), 2992 (2002)
- Chakraborty, V., Mukhopadhyay, B., Basu, P.K.: Performance prediction of an electro absorption modulator at 1550 nm using GeSn/SiGeSn quantum well structure. *Phys. E* **50**, 67–72 (2013)
- Chang, G.E., Chang, C.O.: Tensile-strained Ge/SiGeSn quantum wells for polarization-insensitive electro-absorption waveguide modulators. *IEEE J. Quantum Electron.* **48**(4), 533–541 (2012)
- Chang, S.W., Chuang, S.L.: Theory of optical gain of Ge-Si(x)Ge(y)Sn(1-x-y) quantum-well lasers. *IEEE J. Quantum Electron.* **43**(3), 249–256 (2007)
- Chang, G.E., Chang, S.W., Chuang, S.L.: Strain-balanced Ge_zSn_{1-z}-Si_xGe_ySn_{1-x-y} multiple-quantum-well lasers. *IEEE J. Quantum Electron.* **46**(12), 1813–1820 (2010)
- Chizmeshya, A.V.G., Ritter, C., Tolle, J., Cook, C., Menendez, J., Kouvetakis, J.: Fundamental studies of P(GeH₃)₃, as(GeH₃)₃, and Sb(GeH₃)₃: practical *n*-dopants for new group IV semiconductors. *Chem. Mater.* **18**, 6266–6277 (2006)
- D’Costa, V.R., Cook, C.S., Birdwell, A.G., Littler, C.L., Canonico, M., Zollner, S., Kouvetakis, J., Menendez, J.: Optical critical points of thin-film Ge_{1-y}Sn_y alloys: a comparative Ge_{1-y}Sn_y/Ge_{1-x}Six study. *Phys. Rev. B* **73**(1–16), 125207 (2006)
- D’Costa, V.R., Fang, Y., Mathews, J., et al.: Sn alloying as a means of increasing optical absorption in Ge at the C- and L- telecommunication bands. *Semicond. Sci. Technol.* **24**(1–8), 115006 (2009)
- Deen, M.J., Basu, P.K.: *Silicon Photonics: Fundamentals and Devices*. Wiley, Chichester (2012)
- Frimel, S.M., Roenker, K.P.: A thermionic-field-diffusion model for Npn bipolar heterojunction phototransistors. *J. Appl. Phys.* **82**, 1427–1437 (1997a)
- Frimel, S.M., Roenker, K.P.: Gummel-Poon model for Npn heterojunction bipolar phototransistor. *J. Appl. Phys.* **82**, 3581–3592 (1997b)
- Khan, H.A., Rezazadeh, A.A., Sohaib, S.: Modeling and analysis of the spectral response for AlGaAs/GaAs HPTs for short wavelength optical communication. *J. Appl. Phys.* **109**, 104507 (2011)
- Menendez, J., Kouvetakis, J.: Type-I Ge/GeSiSn strained layer heterostructures with a direct Ge band gap. *Appl. Phys. Lett.* **85**, 1175–1178 (2004)
- Moontragoon, P., Vukmirovic, N., Ikonic, Z., Harrison, P.: SnGe asymmetric quantum well electroabsorption modulators for long-wave silicon photonics. *IEEE J. Sel. Top. Quantum Electron.* **16**(1), 100–105 (2010)
- Oehme, M., Schmid, M., Kaschel, M., Gollhofer, M., Widmann, D., Kasper, E., Schulze, J.: GeSn p-i-n detectors integrated on Si with up to 4% Sn. *Appl. Phys. Lett.* **101**(14), 141110 (2012)
- Park, M.S., Jang, J.H.: Enhancement of optical gain in floating-base InGaP-GaAs heterojunction phototransistors. *IEEE Photonics Technol. Lett.* **22**, 1202–1204 (2010)
- Pavesi, L., Lockwood, D.J. (eds.): *Silicon Photonics*. Springer, New York (2004)
- Roucka, R., Xie, J., Kouvetakis, J., Mathews, J., D’Costa, V., Menendez, J., Tolle, J., Yu, S.Q.: Ge_{1-y}Sn_y photoconductor structures at 1.55 μm : from advanced materials to prototype devices. *J. Vac. Sci. Technol. B* **26**, 1952–1959 (2008)
- Schaevitz, R.K., Edwards, E.H., Roth, J.E., Fei, E.T., Rong, Y., Wahl, P., Kamins, T.I., Harris, J.S., Miller, D.A.: Simple electroabsorption calculator for designing 1310 nm and 1550 nm modulators using germanium quantum wells. *IEEE J. Quantum Electron.* **48**(2), 187–197 (2012)
- Scott, D.C., Fetterman, H.R.: *Indium Phosphide and Related Materials: Processing, Technology and Devices*. In: Katz, A. (ed.), pp. 351–403. Artech House (1995)
- Su, S., Cheng, B., Xue, C., Wang, W., et al.: GeSn p-i-n photodetector for all telecommunication band detection. *Opt. Express* **19**(7), 6400–6405 (2011)
- Sun, G., Soref, R.A., Cheng, H.H.: Design of a Si-based lattice-matched room temperature GeSn/GeSiSn multi-quantum-well mid-infrared laser diode. *Opt. Express* **18**(9), 19957–19965 (2010a)
- Sun, G., Soref, R.A., Cheng, H.H.: Design of an electrically pumped SiGeSn/GeSn/SiGeSn double heterostructure mid infrared laser. *J. Appl. Phys.* **108**, 033107 (2010b)
- Tan, S.H., Chen, H.R., Chen, W.T., Hsu, M.K., Lin, A.H., Lour, W.S.: Characterization and modeling of three-terminal heterojunction phototransistors using an InGaP layer for passivation. *IEEE Trans. Electron Dev.* **52**, 204–210 (2005)
- Zhang, Y., Li, C., Chen, S.Y., Lai, H.K., Kang, J.Y.: Numerical analysis of SiGe heterojunction Bipolar phototransistor based on virtual substrate. *Solid-State Electron.* **52**, 1782–1790 (2008)
- Zhu, Y.H., Xu, Q., Fan, W.J., Wang, J.W.: Theoretical gain of strained GeSn_{0.02}/Ge_{1-x-y}Si_xSn_y quantum well laser. *J. Appl. Phys.* **107**, 073108 (2010)